

New insights in piezoelectric free-vibrations using simplified modeling and analyses

Ayech Benjeddou

*Institut Supérieur de Mécanique de Paris, Structures,
3 rue Fernand Hainaut, 93407 Saint Ouen CEDEX, France*

(Received March 5, 2009, Accepted April 14, 2009)

Abstract. New insights are presented in simplified modeling and analysis of free vibrations of piezoelectric – based smart structures and systems. These consist, first, in *extending* the wide used piezoelectric–thermal analogy (TA) simplified modeling approach in currently static actuation to piezoelectric free–vibrations under short-circuit (SC) and approximate open-circuit (OC) electric conditions; second, the popular piezoelectric strain induced – potential (IP) simplified modeling concept is revisited. It is shown that the IP resulting frequencies are insensitive to the electric SC/OC conditions; in particular, SC frequencies are found to be the same as those resulting from the newly proposed OC TA. Two-dimensional plane strain (PStrain) and plane stress (PStress) free-vibrations problems are then analyzed for above used SC and approximate OC electric conditions. It is shown theoretically and validated numerically that, for both SC and OC electric conditions, PStress frequencies are lower than PStrain ones, and that 3D frequencies are bounded from below by the former and from above by the latter. The same holds for the modal electro-mechanical coupling coefficient that is retained as a comparator of presented models and analyses.

Keywords: piezoelectricity; free-vibration; thermal analogy; induced potential; plane strain; plane stress.

1. Introduction

During the last three decades, piezoelectric materials – based smart structures and systems were the focus of intense fundamental and applied researches (Benjeddou 2004). However, their modeling and analysis still require special research efforts to reach wide acceptance by this technology end-users. Therefore, unavoidably, simplifying the underneath highly coupled equations results in approximate electromechanical coupling and electric boundary conditions (BC) representations.

Piezoelectric electromechanical coupling representations follow mostly practical (engineering) modeling methods like piezoelectric-thermal analogy (TA) (Poizat and Benjeddou 2006), strain higher-order induced potential (IP) (Benjeddou 2002) or strain higher-order induced field (IF) (Krommer 2003a) concepts. The former two approaches have the numerical advantage to avoid additional electric degrees of freedom (DOF) (Benjeddou 2000). Nevertheless, the TA approach represents only the piezoelectric converse effect via a thermal-like induced actuation strain for which the transverse piezoelectric strain constants d_{3q} ($q=1,\dots,6$) replace the thermal expansion coefficients α_q and the transverse electric field E_3 , assumed through-the-thickness constant, replaces the temperature variation θ (Côté, *et al.* 2004, Kim, *et al.* 2008). Moreover, when applied to free-vibrations, the TA can provide only short-circuit (SC) modal

properties (Benjeddou 2008). However, beside the equivalent electric load, resulting from the converse piezoelectric effect, the IP approach represents also the direct piezoelectric effect by partially modifying the piezoelectric elastic constants thanks to the quadratic potential derived from fulfilling an approximate electrostatic charge equation (Benjeddou, *et al.* 1997, Rahmoune, *et al.* 1998) or an approximate (nil transverse electric displacement D_3) open-circuit (OC) electric BC (Brockmann, *et al.* 2006). Therefore, the former has not to be used further in the variational formulation as erroneously done in (Marinkovic, *et al.* 2007); otherwise, the direct effect is double represented. The same representation as the IP is reached by the IF strength of materials-like analytical technique (Krommer 2003a). However, although enhanced by satisfying automatically the electrodes equipotentiality (EP) constraint, the latter leads to non-local generalized constitutive equations which implementation feasibility using local numerical techniques, like the finite element (FE) method, remains to be proved.

For computational cost efficiency and simplicity reasons, piezoelectric-based smart structures and systems are often simulated using two-dimensional (2D), rather than three-dimensional (3D), models. However, for this purpose, most of commercial FE softwares, having piezoelectricity modeling capability, still propose only plane strain (PStrain) and plane stress (PStress) piezoelectric 2D FE (Lin, *et al.* 1994). The latter were used widely for validating theoretical and numerical 2D models for static or dynamic analyses of piezoelectric adaptive structures. Besides, most of early 2D analytical solutions for the free-vibrations analysis of piezoelectric adaptive structures assumed cylindrical bending kinematics (Heyliger and Brooks 1995, Vel, *et al.* 2004, Zhang, *et al.* 2006) or PStrain state (Fernandes and Pouget 2003). These assumptions were also used to reduce 2D piezoelectric adaptive plate models to one dimensional (1D) piezoelectric adaptive beam ones (Shu 2005). In the literature, the latter were simulated using both PStress (Lin, *et al.* 1994, Krommer 2000) and PStrain (Krommer 2003b, Jiang and Li 2008) 2D piezoelectric FE within ANSYS® (Lin, *et al.* 1994) or ABAQUS® (Krommer 2000, Krommer 2003b, Fernandes and Pouget 2003, Vel, *et al.* 2004, Jiang and Li 2008) commercial codes.

This research work aims to present new insights in simplified modeling and analysis of free-vibrations of piezoelectric-based smart structures and systems. Hence, in the following, the wide used piezoelectric TA simplified modeling approach is extended to piezoelectric free-vibrations under SC and approximate OC electric BC; then, the popular piezoelectric IP simplified modeling concept is revisited. Next, simplified 2D PStrain and PStress free-vibrations problems are compared under SC and approximate OC electric BC. These simplified analyses are then linked to the previous simplified modeling approaches. Finally, the resulting theoretical predictions from the proposed simplified models and analyses are validated numerically by analyzing, with ANSYS® FE commercial code, a common piezoelectric smart structure benchmark. For this purpose, the so-called modal electromechanical coupling coefficient (EMCC) is used (a list of abbreviations is provided in Appendix A); it was already shown that it is a good measure of the piezoelectric coupling representation (Deü and Benjeddou 2005).

2. Piezoelectric free-vibrations equations

According to the linear piezoelectricity standards (IEEE 1988), the mechanical equations of a piezoelectric continuum of volume Ω , bounded by a surface S , consist of the body force-free stress equation of motion in Ω , traction-free BC on surface S_T and displacements-free BC on S_u , respectively:

$$\sigma_{ij,j} = \rho \ddot{u}_i \quad (1)$$

$$\sigma_{ij} n_j = 0 \quad (2)$$

$$u_i = 0 \tag{3}$$

where, σ_{ij} ($i, j=1, 2, 3$), u_i and n_j are components of the symmetric Cauchy stress tensor, displacement and outward normal vectors; \ddot{u}_i is the i^{th} acceleration. The summation convention for repeated indices applies throughout.

Electric equations, analogue to those of Eqs. (1-3), are the electrostatic equation for an insulator of volume Ω , the approximate surface charge at an air-dielectric interface of surface S_D , valid for a dielectric constant of the piezoelectric material much larger compared to that of the air (vacuum), and the potential of SC electrodes of surface S_ϕ under zero reference potential:

$$D_{i,i} = 0 \tag{4}$$

$$D_i n_i = 0 \tag{5}$$

$$\phi = 0 \tag{6}$$

where, D_i and ϕ are the electric displacement vector components and potential. It is worthy to recall that on an electroded surface, ϕ must be either specified or some relation given between ϕ and $D_i n_i$. If a pair of electrodes 1 and 2, with area A , operates into a circuit of admittance Y , the condition is (IEEE 1988):

$$I = \int_A \dot{D}_i n_i dA = \pm YV \tag{7}$$

where, the ‘ \pm ’ sign of the current I flowing in the circuit depends on the coordinate axes orientation, and V is the voltage related to the potential difference by: $V = \phi(1) - \phi(2)$. The latter are the potentials on the electrodes surfaces.

Above mechanical motion and electric equilibrium equations are coupled through the following converse and direct piezoelectric constitutive equations, respectively, written using the condensed notations ($p, q=1, \dots, 6; k=1,2,3$):

$$T_p = c_{pq}^E S_q - e_{kp} E_k \tag{8}$$

$$D_i = e_{iq} S_q + \epsilon_{ik}^S E_k \tag{9}$$

where, c_{pq}^E , e_{iq} and ϵ_{ik}^S are, respectively, the stiffness elastic constants at constant electric field (SC), stress piezoelectric constants, and dielectric permittivity at constant strain (blocked). T_p are the engineering stress components ($T_p = \sigma_{ii}, p=i=1,2,3; T_p = \sigma_{ij}, j \neq i, p=9-(i+j)$); S_q, E_k are the engineering strain and electric field components given, respectively, by:

$$S_q = u_{i,i}, q = i = 1, 2, 3 \text{ (no sommation)} \tag{10}$$

$$S_q = u_{i,j} + u_{j,i}, j \neq i, q = 9 - (i + j)$$

$$E_k = -\phi_{,k} \tag{11}$$

Alternative forms to the (S, E) or e -form of Eqs. (8,9) are:

- The (T, E) or d -form given by:

$$S_p = s_{pq}^E T_q + d_{kp} E_k \tag{12}$$

$$D_i = d_{iq} T_q + \epsilon_{ik}^T E_k \tag{13}$$

with, s_{pq}^E , d_{iq} , ϵ_{ik}^T the elastic compliances at constant electric field (SC), strain piezoelectric constants, and dielectric permittivity constants at constant stress (free). These constants ($r=1,\dots,6$) are generally used to find those of Eqs. (8, 9):

$$c_{pr}^E s_{qr}^E = \delta_{pq} \quad (14)$$

$$e_{ip} = d_{iq} c_{qp}^E \quad (15)$$

$$\epsilon_{ij}^S = \epsilon_{ij}^T - d_{iq} e_{jq} \quad (16)$$

- The (T, D) or g -form given by:

$$S_p = s_{pq}^D T_q + g_{kp} D_k \quad (17)$$

$$E_i = -g_{iq} T_q + \beta_{ik}^T D_k \quad (18)$$

where, s_{pq}^D , g_{iq} , β_{ik}^T are, respectively, the elastic compliance constants at constant electric displacement (OC), strain charge piezoelectric constants, and dielectric impermeabilities at constant stress (free). These constants can be obtained from those of Eqs. (12, 13) using these relations:

$$\beta_{ik}^T \epsilon_{jk}^T = \delta_{ij} \quad (19)$$

$$g_{ip} = \beta_{ik}^T d_{kp} \quad (20)$$

$$s_{pq}^D = s_{pq}^E - d_{kp} g_{kq} \quad (21)$$

- The (S, D) or h -form given by:

$$T_p = c_{pq}^D S_q - h_{kp} D_k \quad (22)$$

$$E_i = -h_{iq} S_q + \beta_{ik}^S D_k \quad (23)$$

where, c_{pq}^D , h_{iq} , β_{ik}^S are, respectively, the elastic stiffness constants at constant electric displacement (OC), stress charge piezoelectric constants, and dielectric impermeabilities at constant strain (blocked). They can be obtained from those of Eqs. (17, 18) by these relations:

$$c_{pr}^D s_{qr}^D = \delta_{pq} \quad (24)$$

$$h_{ip} = g_{iq} c_{qp}^D \quad (25)$$

$$\beta_{ij}^S = \beta_{ij}^T - g_{iq} h_{jq} \quad (26)$$

It is worthy to notice that piezoelectric materials manufacturers provide only incomplete data sets of mainly Eq. (12, 13) and few of those of Eqs. (17, 18, 22, 23). It is then necessary to complete manufacturers' data prior to any numerical simulation depending on the available constants; a simple procedure is described in (Chevallier, *et al.* 2008). However, the classical mechanical displacement-potential based

piezoelectric FE formulations use primarily the constitutive relations of Eqs. (8, 9), while the mechanical displacement-charge based piezoelectric hybrid FE ones use Eqs. (22, 23). Besides, commercial FE codes with piezoelectric modeling capability have implemented only the classical displacement-potential formulations. Hence, the latter can be written for above Eqs. (1-6) as:

$$\int_{\Omega} \delta S_p T_p d\Omega - \int_{\Omega} \delta E_i D_i d\Omega + \int_{\Omega} \delta u_i \rho \ddot{u}_i d\Omega = 0 \quad (27a)$$

where, T_p and D_i are related by the SC constitutive relations of Eqs. (8, 9), and ρ is the material mass density.

For harmonic free-vibrations of circular frequency ω , Eq. (27a) becomes:

$$\int_{\Omega} \delta S_p T_p d\Omega - \int_{\Omega} \delta E_i D_i d\Omega - \omega^2 \int_{\Omega} \delta u_i \rho u_i d\Omega = 0 \quad (27b)$$

For mechanical displacement and electric displacement dependent formulations, analogue relations to Eqs. (27a, 27b) are respectively:

$$\int_{\Omega} \delta S_p T_p d\Omega + \int_{\Omega} \delta D_i E_i d\Omega + \int_{\Omega} \delta u_i \rho \ddot{u}_i d\Omega = 0 \quad (28a)$$

$$\int_{\Omega} \delta S_p T_p d\Omega + \int_{\Omega} \delta D_i E_i d\Omega - \omega^2 \int_{\Omega} \delta u_i \rho u_i d\Omega = 0 \quad (28b)$$

As mentioned earlier, Eqs. (27a, 27b) have to use the constitutive Eqs. (8, 9), while Eqs. (28a, 28b) have to use Eqs. (22, 23).

3. Simplified modeling of piezoelectric free-vibrations

The TA approach is first extended to charge-driven actuation problems thanks to the OC converse piezoelectric constitutive relation of Eq. (22). Then, the strain IP concept, derived both from the approximate electrostatic equation and the approximate OC BC, is revisited and linked to the classical and extended TA approaches.

3.1. Extension of the piezoelectric-thermal analogy approach

Thanks to Eqs. (14, 15), the converse constitutive relation of Eq. (8) can be transformed into the following thermoelastic-like constitutive equation (Benjeddou 2000):

$$T_p = c_{pq}^E (S_q - \Lambda_q^E) \quad (29)$$

with,

$$\Lambda_q^E = d_{iq} E_i \quad (30)$$

But, in order to reach full piezoelectric-thermal analogy ($\Lambda_q^{th} = \alpha_q \theta$) the classical through-the-thickness (usually along axis 3) linear and in-plane uniform electric potential assumptions have to be made so that the following electric field simplification holds:

$$E_1 = E_2 = 0, E_3 = \frac{V}{h} \quad (31)$$

where, V denotes the actuation voltage across the piezoelectric thickness h . These relations provide $\delta E_i = 0$ and $\Lambda_q^E = d_{3q} E_3$ (TA: $\alpha_q \rightarrow d_{3q}$, $\theta \rightarrow E_3$). With the latter and after combining Eq. (29-31) with Eq. (15), Eq. (27a) simplifies to this voltage-driven actuation problem:

$$\int_{\Omega} \delta S_p c_{pq}^E S_q d\Omega + \int_{\Omega} \delta u_i \rho \ddot{u}_i d\Omega = \int_{\Omega} \delta S_p e_{3p} E_3 d\Omega = \int_{\Omega} \delta S_p \frac{e_{3p}}{h} V d\Omega \quad (32)$$

When reduced to the static case, Eq. (32) provides the classical voltage-driven static actuation problem:

$$\int_{\Omega} \delta S_p c_{pq}^E S_q d\Omega = \int_{\Omega} \delta S_p \frac{e_{3p}}{h} V d\Omega \quad (33)$$

Since for SC electrodes $V=0$, Eq. (32) reduces to this harmonic free-vibrations problem of circular frequency ω_E :

$$\int_{\Omega} \delta S_p c_{pq}^E S_q d\Omega - \Omega_E^2 \int_{\Omega} \delta u_i \rho u_i d\Omega = 0 \quad (34)$$

from which the SC (super/subscript E) modal properties can be extracted. It is worthy to notice that TA, as in Eq. (34), was not used before for modal analysis. Hence it can be considered as new.

Similarly to Eq. (29), Eq. (22) can be transformed, thanks to Eqs. (24, 25), into the following thermoelastic-like constitutive equation:

$$T_p = c_{pq}^D (S_q - \Lambda_q^D) \quad (35)$$

with,

$$\Lambda_q^D = g_{iq} D_i \quad (36)$$

and

$$c_{pq}^D = c_{pq}^E + e_{ip} \beta_{ij}^S e_{jq} \quad (37)$$

obtained from the condensation of E_k between Eqs. (8) and (9). This full OC elastic matrix is given explicitly in Eq. (B3) of Appendix B.

Again, in order to reach full piezoelectric-thermal analogy ($\Lambda_q^{th} = \alpha_q \theta$) through-the-thickness (usually along axis 3) *constant* and in-plane *uniform* electric displacement assumptions (Rahmoune, *et al.* 1998) have to be made so that the following electric displacement simplification holds:

$$D_1 = D_2 = 0, D_3 = \frac{Q}{A} \quad (38)$$

where, Q is the imposed surface charge on the electrode of area A . These relations provide $\delta D_i = 0$ and $\Lambda_q^D = g_{3q} D_3$ (TA: $\alpha_q \rightarrow g_{3q}$, $\theta \rightarrow D_3$). With the latter and after combining Eqs. (35, 36, 38) with Eq. (25), Eq. (28a) simplifies to this new charge-driven actuation problem:

$$\int_{\Omega} \delta S_p \bar{c}_{pq}^D S_q d\Omega + \int_{\Omega} \delta u_i \rho \ddot{u}_i d\Omega = \int_{\Omega} \delta S_p \frac{h_{3p}}{A} Q d\Omega \quad (39)$$

with,

$$\bar{c}_{pq}^D = c_{pq}^E + e_{3p} \beta_{33}^S e_{3q} \quad (40)$$

obtained by considering $i=j=3$ in Eq. (37) thanks to Eq. (38). The explicit expression of this reduced OC

elastic matrix is given in Eq. (B4) of Appendix B. Its comparison with the full one of Eq. (37) indicates that it differs by the transverse shear elastic constants which are modified in the latter but not in the former. It can then be concluded that, for thin piezoelectric patches, where the transverse shear behavior is not much influent, the unidirectional constant electric displacement assumption, given in Eq. (38), is acceptable (Rahmoune, *et al.* 1998). Compared to the corresponding SC elastic constants (see Eq. (B1) of Appendix B), the other OC ones are modified except for the in-plane shear constant which remains unmodified. Besides, since $e_{33}, \epsilon_{33}^S > 0$ and $e_{31}, e_{32} < 0$ (see Eq. (B2) of Appendix B), all elastic constants of both matrices are increased except the 1-3 and 2-3 shear plane ones (upper two terms of the 3rd column) which are reduced (see the application to the PZT-5A material in Appendix C). It can then be expected that this stiffness reduction shall influence 3D and 2D PStress analyses but not PStrain ones (normal transverse strain vanishes in this case). Since the mass does not depend on the strain/stress assumptions, PStrain OC frequencies are then expected higher than the 3D and 2D PStress ones; this is an interesting new theoretical result that will be confirmed later in the next section.

When reduced to the static case, Eq. (39) provides this new charge-driven static actuation problem:

$$\int_{\Omega} \delta S_p \bar{c}_{pq}^D S_p d\Omega = \int_{\Omega} \delta S_p \frac{h_{3q}}{A} Q d\Omega \quad (41)$$

Since for OC electrodes $Q=0$, Eq. (39) reduces to this harmonic free-vibrations problem of circular frequency $\bar{\omega}_D$:

$$\int_{\Omega} \delta S_p \bar{c}_{pq}^D S_p d\Omega - \bar{\omega}_D^2 \int_{\Omega} \delta u_i \rho u_i d\Omega = 0 \quad (42)$$

from which approximate OC (super/subscript D) modal properties can be extracted.

The last two equations are new and can be seen as extensions of the TA which could not be used earlier for charge-driven actuation and approximate OC free-vibrations analysis. Hence, the TA based squared EMCC can be evaluated approximately after post-treating the solutions of Eqs. (34, 42) as follows:

$$K_{TA}^2 = \frac{\bar{\omega}_D^2 - \omega_E^2}{\omega_E^2} \quad (43)$$

3.2. Revisit of the piezoelectric induced potential concept

Under unidirectional transverse electric displacement assumption ($D_1=D_2=0$), the electrostatic equilibrium of Eq. (4) reduces to the following relation after substituting the corresponding direct constitutive equation from Eq. (9) for an orthotropic piezoelectric material:

$$D_{3,3} = e_{3q} S_{q,3} + \epsilon_{33}^S E_{3,3} = 0 \quad (44)$$

Notice that, at this stage, no need for any assumption on the electric field.

Taking the primitive of the electric displacement derivative from Eq. (44) provides this expression for the transverse electric field:

$$E_3 = -(\epsilon_{33}^S)^{-1} e_{3q} S_q + \bar{E}_3 = -\beta_{33}^S e_{3q} S_q + \bar{E}_3 \quad (45)$$

where, \bar{E}_3 is a constant of integration that can be defined from the electrodes BC. The first term in the

right-hand-side of Eq. (45) is the so-called induced electric field (Krommer 2003a) which is through-thickness linear for linear strains; after its thickness integration, it gives a quadratic induced electric potential, playing the role of a stiffening effect (SE) (Benjeddou, *et al.* 1997, Rahmoune, *et al.* 1998, Al-Ajmi and Benjeddou 2008).

Substituting back this relation in the converse constitutive relation of Eq. (8), but for a unidirectional transverse electric field ($E_1=E_2=0$), provides:

$$T_p = (c_{pq}^E + e_{3p}\beta_{33}^S e_{3q})S_q - e_{3p}\bar{E}_3 = \bar{c}_{pq}^D S_q - e_{3p}\bar{E}_3 = \bar{c}_{pq}^D (S_q - \bar{\Lambda}_q^E), \bar{\Lambda}_q^E = d_{3p}\bar{E}_3 \quad (46)$$

It is worthy to notice that the last relation of Eq. (46) is a thermo-elastic like one that uses the reduced OC elastic matrix of Eq. (40). The second term in the brackets of the first equality of Eq. (46) represents the piezoelectric coupling SE.

With the unidirectional electric displacement assumption and the electrostatic equilibrium (fulfilled a priori) of Eq. (44), the variational formulation of Eq. (27a) reduces to the following pure mechanical one:

$$\int_{\Omega} \delta S_p T_p d\Omega + \int_{\Omega} \delta u_i \rho \ddot{u}_i d\Omega = 0 \quad (47)$$

where, T_p is given by Eq. (46); hence, Eq. (47) can be written explicitly as:

$$\int_{\Omega} \delta S_p \bar{c}_{pq}^D S_q d\Omega + \int_{\Omega} \delta u_i \rho \ddot{u}_i d\Omega = \int_{\Omega} \delta S_p e_{3p} \bar{E}_3 d\Omega \quad (48)$$

This IP actuation problem generalizes the 1D available one (Benjeddou, *et al.* 1997).

In the static case, Eq. (48) reduces to this voltage-driven actuation problem:

$$\int_{\Omega} \delta S_p \bar{c}_{pq}^D S_q d\Omega = \int_{\Omega} \delta S_p e_{3p} \bar{E}_3 d\Omega \quad (49)$$

This is the same as that available for piezoelectric plates (Rahmoune, *et al.* 1998).

From Eqs. (48, 49), it can be noticed that a TA potential-driven actuation problem is obtained but with the reduced stiffness matrix of Eq. (40). Hence, the IP effect can be simulated using the TA concept; this is a new finding in the sense that there is no need for developing piezoelectric FE without electric DOF; in fact, commercial codes can be used without extra effort for implementing Eqs. (48, 49).

Since for SC electrodes $\bar{E}_3 = 0$, Eq. (48) reduces to this harmonic free-vibrations problem of circular frequency $\bar{\omega}_E$:

$$\int_{\Omega} \delta S_p \bar{c}_{pq}^D S_q d\Omega - \bar{\omega}_E^2 \int_{\Omega} \delta u_i \rho u_i d\Omega = 0 \quad (50)$$

from which associate SC modal properties can be extracted. This equation proves, for the first time here, that the IP SC free-vibration problem is equivalent to that of the newly proposed OC TA of Eq. (42). In particular, SC IP eigenvalues are in fact OC TA ones; i.e.:

$$\bar{\omega}_E^2 = \bar{\omega}_D^2 \quad (51)$$

Hence, the EMCC can be also approximated using the IP concept using Eq. (43) but with ω_E^2 calculated after dropping the SE, of Eq. (46), due to the strain IP:

$$K_{IP}^2 = \frac{\bar{\omega}_E^2 - \omega_E^2}{\omega_E^2} \quad (52)$$

Let's now consider the following asymptotic Neumann problem of a thin piezoelectric medium (see for example Rahmoune, *et al.* 1998):

$$D_{3,3} = 0 \text{ in } \Omega \quad (53)$$

$$D_3 = 0 \text{ on } S_D \quad (54)$$

This has the following trivial solution for an orthotropic piezoelectric material:

$$D_3 = e_{3q} S_q + \epsilon_{33}^S E_3 = 0 \quad (55)$$

Extracting the transverse field from this relation provides:

$$E_3 = -(\epsilon_{33}^S)^{-1} e_{3q} S_q = -\beta_{33}^S e_{3q} S_q \quad (56)$$

Substituting back this relation in the converse constitutive relation of Eq. (8), but for a unidirectional transverse electric field ($E_1=E_2=0$), provides:

$$T_p = (c_{pq}^E + e_{3p} \beta_{33}^S e_{3q}) S_q = \bar{c}_{pq}^D S_q \quad (57)$$

It can be easily demonstrated that the free-vibrations problem associated to Eqs. (53, 54, 57) should be the same as the new OC TA one given in Eq. (42). Hence, under unidirectional transverse electric displacement and field assumptions, the IP quadratic term derived from the approximate electrostatic equation only, as in Eq. (44), or the electric displacement-free BC only, as in Eq. (55), is the same. This result can be noticed also from derivations in (Brockmann, *et al.* 2006). More interesting is the fact that the IP-based free-vibrations problems are insensitive to the electric BC i.e. SC and OC free-vibrations problems provide the same modal properties since Eqs. (42) and Eq. (50) are the same. This result has been also noticed in (Al-Ajmi and Benjeddou 2008).

It is worthy to emphasize that:

- Both TA and IP approaches do not use electric potential independent variables; hence, they are suitable for actuation or free-vibration only. The sensing case has to be handled separately via Eq. (53) or (54) but requires the consideration of the EP constraint, which is an open question for FEs that do not have electric DOF.

- Consequently, these simplified models can not consider numerically the EP constraint although it has been reached analytically as in (Krommer 2003a) for example. Therefore, to implement the EP condition, it is easier and recommended to introduce nodal/elemental electric potential DOF on the electrodes.

- Since the electrostatic charge equation is fulfilled exactly for the IP concept, its use again in the weak variational formulation, as in (Marinkovic, *et al.* 2007), is erroneous since it consists of a double representation of the direct effect.

- Above reduced OC elastic constants are in fact incomplete OC ones, as shown in Eq. (B4) of Appendix B, since the elastic constants were modified only with regards to the transverse components related to the IF. They should be enough for a uniform electric potential that leads to a constant electric field.

- The popular nil transverse electric displacement does not represent a true OC electric BC but an air-dielectric interface; i.e. non electroded (NE) interface (see Eq. (7) for the true OC electric condition according to (IEEE 1988)).

4. Simplified analyses of piezoelectric free-vibrations

Most of FE commercial codes impose that the 2D work plane, for PStrain and PStress analyses, is the x-y plane; for piezoelectric thin structures, this imposes that the piezoelectric patch thickness, hence polarization, is along the y-axis. The matrices of the standard (with the polarisation along axis 3) piezoelectric constitutive Eqs. (B1, B2) have to be rotated so that the poling direction lies along the material axis 2; above converse and direct constitutive relations of Eqs. (8,9) become then:

$$\begin{Bmatrix} T_1 \\ T_2 \\ T_3 \\ T_4 \\ T_5 \\ T_6 \end{Bmatrix} = \begin{bmatrix} c_{11} & c_{13} & c_{12} & 0 & 0 & 0 \\ c_{13} & c_{33} & c_{23} & 0 & 0 & 0 \\ c_{12} & c_{23} & c_{22} & 0 & 0 & 0 \\ 0 & 0 & 0 & c_{44} & 0 & 0 \\ 0 & 0 & 0 & 0 & c_{66} & 0 \\ 0 & 0 & 0 & 0 & 0 & c_{55} \end{bmatrix}^E \begin{Bmatrix} S_1 \\ S_2 \\ S_3 \\ S_4 \\ S_5 \\ S_6 \end{Bmatrix} - \begin{bmatrix} 0 & e_{31} & 0 \\ 0 & e_{33} & 0 \\ 0 & e_{32} & 0 \\ 0 & 0 & e_{24} \\ 0 & 0 & 0 \\ e_{15} & 0 & 0 \end{bmatrix} \begin{Bmatrix} E_1 \\ E_2 \\ E_3 \end{Bmatrix} \quad (58)$$

$$\begin{Bmatrix} D_1 \\ D_2 \\ D_3 \end{Bmatrix} = \begin{bmatrix} 0 & 0 & 0 & 0 & 0 & e_{15} \\ e_{31} & e_{33} & e_{32} & 0 & 0 & 0 \\ 0 & 0 & 0 & e_{24} & 0 & 0 \end{bmatrix} \begin{Bmatrix} S_1 \\ S_2 \\ S_3 \\ S_4 \\ S_5 \\ S_6 \end{Bmatrix} + \begin{bmatrix} \epsilon_{11} & 0 & 0 \\ 0 & \epsilon_{33} & 0 \\ 0 & 0 & \epsilon_{22} \end{bmatrix}^S \begin{Bmatrix} E_1 \\ E_2 \\ E_3 \end{Bmatrix} \quad (59)$$

Here after, these equations will be simplified for 2D PStrain and PStress states, associate free-vibrations problems will be derived and expected resulting frequencies and post-treated modal EMCC will be theoretically predicted and compared.

4.1. Plane strain 2D analysis

For a piezoelectric patch electroded on its upper and lower major surfaces, the piezoelectric PStrain behavior assumes nil transverse strains and unidirectional (along the polarization) electric field:

$$S_3 = S_4 = S_5 = 0, E_1 = E_3 = 0 \quad (60a,b)$$

Substituting these relations in Eqs. (58, 59) reduces them to the following ones:

$$\begin{Bmatrix} T_1 \\ T_2 \\ T_6 \\ D_2 \end{Bmatrix} = \begin{bmatrix} c_{11}^E & c_{13}^E & 0 & -e_{31} \\ c_{13}^E & c_{33}^E & 0 & -e_{33} \\ 0 & 0 & c_{55}^E & 0 \\ e_{31} & e_{33} & 0 & \epsilon_{33}^S \end{bmatrix} \begin{Bmatrix} S_1 \\ S_2 \\ S_6 \\ E_2 \end{Bmatrix} \quad (61)$$

$$T_3 = c_{12}^E S_1 + c_{23}^E S_2 - e_{32} E_2, \quad T_4 = T_5 = 0, \quad D_1 = e_{15} S_6, \quad D_3 = 0 \quad (62)$$

From Eq. (62), notice that the normal transverse stress and axial electric displacement are non nil; however, since their duals are nil, as in Eq. (60), they shall not contribute to the electromechanical enthalpy; hence, due to Eqs. (60, 62), the harmonic free-vibrations problem of Eq. (27b) reduces to ($I=1,2,6; \alpha=1,2$):

$$\int_{\Omega} \delta S_I T_I d\Omega - \int_{\Omega} \delta E_2 D_2 d\Omega - \omega^2 \int_{\Omega} \delta u_{,\alpha} \rho u_{,\alpha} d\Omega = 0 \quad (63)$$

where, T_I and D_2 are defined by Eq. (61).

Consider now again the assumption of through-the-thickness linear electric potential that leads to a constant electric field E_2 . In this case, the 2D SC ($E_2=0$) free-vibrations problem of Eq. (63) reduces to this pure elastic one:

$$\int_{\Omega} \delta S_I T_I d\Omega - \omega^2 \int_{\Omega} \delta u_{,\alpha} \rho u_{,\alpha} d\Omega = 0 \quad (64)$$

with,

$$\begin{Bmatrix} T_1 \\ T_2 \\ T_6 \end{Bmatrix} = \begin{bmatrix} c_{11}^E & c_{13}^E & 0 \\ c_{13}^E & c_{33}^E & 0 \\ 0 & 0 & c_{55}^E \end{bmatrix} \begin{Bmatrix} S_1 \\ S_2 \\ S_6 \end{Bmatrix} \quad (65)$$

From Eqs. (64, 65), it can be concluded that the SC frequencies are similar to the pure elastic ones. The piezoelectric effect is then non visible under SC electric conditions; it is present only with its passive (mass and elastic stiffness) effect.

If now the transverse electric displacement is assumed through-the-thickness constant and in-plane uniform, $D_2=0$ approximates an OC electric condition and the corresponding free-vibrations problem is as in Eq. (64) but with the following elastic constants that are modified from Eq. (61) by the OC electric condition ($D_2=0$):

$$\begin{Bmatrix} T_1 \\ T_2 \\ T_6 \end{Bmatrix} = \begin{bmatrix} c_{11}^D & c_{13}^D & 0 \\ c_{13}^D & c_{33}^D & 0 \\ 0 & 0 & c_{55}^E \end{bmatrix} \begin{Bmatrix} S_1 \\ S_2 \\ S_6 \end{Bmatrix} \quad (66)$$

with,

$$c_{11}^D = c_{11}^E + \frac{e_{31}^2}{\epsilon_{33}^S}, \quad c_{13}^D = c_{13}^E + \frac{e_{31}e_{33}}{\epsilon_{33}^S}, \quad c_{33}^D = c_{33}^E + \frac{e_{33}^2}{\epsilon_{33}^S} \quad (67)$$

Since all SC elastic constants are positive, e_{31} is negative, e_{33} and ϵ_{33}^S are positive, c_{11}^D and c_{33}^D are increased, while c_{13}^D is decreased (see Appendix C for a PZT-5A material example). Hence, since the mass does not depend on the strain/electric displacement assumptions, OC frequencies are expected to be higher than SC ones; also, it is expected that the PStrain frequencies are higher than 3D ones. Besides, since the x - y in-plane shear stiffness c_{55}^E is unmodified by the OC condition, x - y in-plane shear (torsion) modes are expected to be uncoupled. These comments are consistent with those provided after Eq. (40). Eqs. (66, 67) are also consistent with the reduced OC elastic matrix detailed in Eq. (B4) of Appendix B since they share the same unidirectional and constant electric field and displacement assumptions.

It is worthwhile to emphasize that previous interpretations do not take into account the EP constraint

effect since the approximate OC free-vibrations problem of Eq. (64) has no longer electric variables on which this condition has to be applied.

4.2. Plane stress 2D analysis

For a piezoelectric patch electroded on its upper and lower major surfaces, the piezoelectric PStress behavior assumes nil transverse stresses and unidirectional electric field (along the polarization):

$$T_3 = T_4 = T_5 = 0, E_1 = E_3 = 0 \quad (68a,b)$$

Substituting these relations in Eqs. (58, 59) reduces them to the following ones:

$$\begin{Bmatrix} T_1 \\ T_2 \\ T_6 \\ D_2 \end{Bmatrix} = \begin{bmatrix} -E & -E & - & - \\ c_{11} & c_{13} & 0 & -e_{31} \\ -E & -E & - & - \\ c_{13} & c_{33} & 0 & -e_{33} \\ 0 & 0 & c_{55}^E & 0 \\ - & - & - & - \\ e_{31} & e_{33} & 0 & \epsilon_{33}^S \end{bmatrix} \begin{Bmatrix} S_1 \\ S_2 \\ S_6 \\ E_2 \end{Bmatrix} \quad (69)$$

$$S_3 = \frac{1}{c_{22}^E} (e_{32} E_2 - c_{12}^E S_1 - c_{23}^E S_2), S_4 = S_5 = 0, D_1 = e_{15} S_6, D_3 = 0 \quad (70)$$

From Eq. (70), notice that the normal transverse strain and axial electric displacement are non nil; however, since their conjugates are nil, as in Eq. (68), they shall not contribute to the electromechanical enthalpy. Hence, due to Eqs. (68, 70), the 2D variational equation of the harmonic free-vibrations remains as in Eq. (64). In Eq. (69), the reduced (modified) elastic stiffness, piezoelectric and dielectric constants are given by:

$$\bar{c}_{11}^E = c_{11}^E - \frac{c_{12}^{E^2}}{c_{22}^E}, \quad \bar{c}_{13}^E = c_{13}^E - \frac{c_{12}^E c_{23}^E}{c_{22}^E}, \quad \bar{c}_{33}^E = c_{33}^E - \frac{c_{23}^{E^2}}{c_{22}^E} \quad (71)$$

$$\bar{e}_{31} = e_{31} - e_{32} \frac{c_{12}^E}{c_{22}^E}, \quad \bar{e}_{33} = e_{33} - e_{32} \frac{c_{23}^E}{c_{22}^E}, \quad \bar{\epsilon}_{33}^S = \epsilon_{33}^S + \frac{e_{32}^2}{c_{22}^E} \quad (72)$$

Notice that the modified elastic constants in Eq. (71) are different from OC ones of Eq. (67). Since all elastic constants are positive, it can be also noticed that the PStress modified stiffness constants are lower than those of the PStrain ones of Eq. (65) (See appendix C for a PZT-5A material example). Since the mass is independent of the strain/stress assumptions, it is then expected that the PStress SC frequencies are lower than PStrain ones. This result was already observed from FE analysis (Wang 2004). Besides, from Eq. (71), it is expected that PStress SC frequencies are lower than 3D ones. Hence, it can be concluded that 3D SC frequencies are bounded from below by the PStress ones and from above by the PStrain ones.

On the other hand, since e_{31} and e_{32} are negative while e_{33} is positive, Eq. (72) indicates that the corresponding modified constants are decreased (\bar{e}_{31}) and increased (\bar{e}_{33}), respectively. Moreover, since the transverse dielectric constant is positive, the PStress modified dielectric one ($\bar{\epsilon}_{33}^S$) is increased compared to the PStrain one in Eq. (61). These predictions are confirmed by the numerical values of the PZT-5A material detailed in Appendix C.

As for the PStrain case, consider now the simple case of through-the-thickness linear electric potential

which leads to $E_2=0$ as the SC electric condition; the corresponding free-vibrations problem reduces then to the pure elastic one of Eq. (64), but with the following constitutive equations:

$$\begin{Bmatrix} T_1 \\ T_2 \\ T_6 \end{Bmatrix} = \begin{bmatrix} -E & -E & 0 \\ c_{11} & c_{13} & 0 \\ -E & -E & 0 \\ c_{13} & c_{33} & 0 \\ 0 & 0 & c_{55}^E \end{bmatrix} \begin{Bmatrix} S_1 \\ S_2 \\ S_6 \end{Bmatrix} \quad (73)$$

The same comment, as that given after Eq. (65) applies also here.

If now the transverse electric displacement is assumed through-thickness constant and in-plane uniform, $D_2=0$ approximates an OC electric condition and the corresponding free-vibrations problem is the same as in Eq. (64) but with the following elastic constants modified from Eq. (69) by the OC condition ($D_2=0$):

$$\begin{Bmatrix} T_1 \\ T_2 \\ T_6 \end{Bmatrix} = \begin{bmatrix} -D & -D & 0 \\ c_{11} & c_{13} & 0 \\ -D & -D & 0 \\ c_{13} & c_{33} & 0 \\ 0 & 0 & c_{55}^E \end{bmatrix} \begin{Bmatrix} S_1 \\ S_2 \\ S_6 \end{Bmatrix} \quad (74)$$

with,

$$c_{11}^{-D} = c_{11}^{-E} + \frac{\bar{e}_{31}^2}{\bar{\epsilon}_{33}^{-S}}, \quad c_{13}^{-D} = c_{13}^{-E} + \frac{\bar{e}_{31}\bar{e}_{33}}{\bar{\epsilon}_{33}^{-S}}, \quad c_{33}^{-D} = c_{33}^{-E} + \frac{\bar{e}_{33}^2}{\bar{\epsilon}_{33}^{-S}} \quad (75)$$

Since all SC elastic modified constants are decreased by the PStress assumptions, \bar{e}_{31} is decreased and, \bar{e}_{33} and $\bar{\epsilon}_{33}^{-S}$ are increased (see comment after Eq. (72)), all OC PStress constants of Eq. (75) are decreased compared to PStrain ones of Eq. (66). Hence, PStress OC frequencies are expected to be lower than PStrain ones; besides, Eq. (75) indicates that the PStress OC constants were reduced two times: first due to the PStress assumptions, second due to the OC electric condition (see Appendix C for numerical values of a PZT-5A material example). Hence they are lower than the 3D initial constants of Eq. (58). It can then be expected that PStress OC frequencies should be lower than 3D ones.

Now combining SC and OC PStress and PStrain predictions regarding the expected SC/OC frequencies, it can be deduced that the 3D modal EMCC is bounded from above by PStrain one and from below by PStress one. This is a very interesting new theoretical result. It will be confirmed later in the validation section.

Notice that, without reducing the importance of these new theoretical results, the same limitations of these interpretations, as those given above at the end of the previous sub-section, shall apply also here.

5. Relations between simplified models and analyses

This section aims to relate the 2D SC and OC elastic matrices resulting from the PStrain and PStress simplified analyses, derived in the previous section, to the 3D ones resulting from the simplified models derived in section 3. Hence, from the comparison of these matrices, the following observations can be made:

- The reduced SC and OC 2D PStrain elastic matrices, given in Eqs. (65) and (66) respectively, can

be obtained from the 3D ones, given in Eqs. (58) and (B4) respectively, by applying the PStrain mechanical assumptions only (Eq. (60a)); i.e., by simply removing 3rd, 4th and 5th columns and rows of Eqs. (58, B4).

- The reduced SC and OC 2D PStress elastic matrices, given in Eqs. (73) and (74) respectively, can be obtained from the 3D ones, given in Eqs. (58) and (B4) respectively, by applying the PStress mechanical assumptions only (Eq. (68a)).

- The reduced OC 2D PStrain and PStress elastic matrices, given in Eqs. (66) and (74) respectively, result from the reduction of the reduced TA/IP-based OC matrix given in Eq. (B4) and not from the full OC one given in Eq. (B3). This can be explained by the fact that 3D TA/IP-based and 2D PStrain/PStress OC matrices derivations share the same unidirectional electric field assumption.

The numerical values of above 3D and 2D SC and OC elastic matrices given in Appendix C for the PZT-5A piezoceramic material confirm the previous observations. Besides, the last observation makes the link between the 3D TA/IP simplified models and the 2D PStrain/PStress simplified analyses. This link gives a new and additional theoretical importance to the thermal analogy simplified modeling approach that has to be validated using FE analyses of a piezoelectric adaptive structure; this is the objective of the subsequent section.

6. Numerical assessments and validations

This section aims first to assess the TA-based EMCC evaluation via Eq. (43) against the SC/OC based EMCC definitions without, similar to a NE condition, or with the consideration of the EP constraint, respectively:

$$K_{NE}^2 = \frac{\omega_{NE}^2 - \omega_E^2}{\omega_E^2} \quad (76)$$

$$K_{EP}^2 = \frac{\omega_{EP}^2 - \omega_E^2}{\omega_E^2} \quad (77)$$

Then, using Eq. (77), the 2D PStrain and PStress EMCC evaluations are assessed with regards to the 3D ones.

Hence, the smart structure benchmark, shown in Fig. 1, consisting of a cantilever Aluminum (Young's modulus of 73 GPa, Poisson's ratio of 0.33 and mass density of 2790 Kg/m³) with attached two pairs of big PZT-5A patches (see Appendix C for PZT-5A properties) is used for the numerical validations of the above derived predictions. Since the early nineties (Hagood, *et al.* 1990, Hagood and von Flowtow

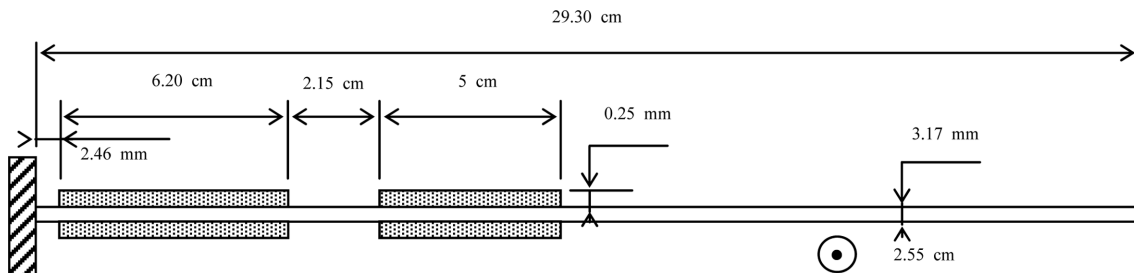


Fig. 1 Benchmark for piezoelectric vibrations using simplified modeling and analyses

1991), this example continues to be very used for benchmarking shunted damping applications (Thornburgh and Chattopadhyay 2001, Benjeddou and Ranger 2006) and EMCC evaluations (Collet and Cunefare 2008).

The benchmark is modeled and analyzed using the ANSYS® FE commercial code. For the 3D analysis, the beam and each patch are meshed, respectively, with 57x15x5 and 15x5x3 SOLID5 piezoelectric FE along x (length), y (width) and z (thickness) axes, leading to a total of 8100 FE. The Extra Shape Functions (ESF) option of the SOLID5 FE was activated in order to avoid any numerical locking. For the comparison coherence, the length (x) x thickness (y -axis for the 2D analysis) 3D mesh is kept the same for the 2D analyses. For all 3D and 2D SC and OC analyses, the interfaces between the patches and beam were kept grounded. The first 10 modes were extracted using the Block Lanczos algorithm and the associated frequencies and post-treated EMCC from Eqs. (43,76,77), corresponding to the transverse bending modes only, are given for the 3D analyses in Table 1 and Fig. 2, respectively.

Table 1 shows that the obtained TA-based approximate OC frequencies are almost similar to the NE ones, which do not consider the EP constraint, and are very close to the OC ones, with the EP constraint, which are the reference. The same is true for TA and NE-based squared EMCC but not for the EP-based ones. The latter are affected by the EP constraint more than the frequencies in the sense that they are decreased by the EP constraint in particular for higher modes.

The 2D PStrain and PStress computed frequencies and corresponding post-treated EMCC from Eq. (77) are given in Table 2 and Fig. 3, respectively. The latter confirm clearly the theoretical predictions in the sense that 3D SC and OC frequencies, as well as squared EMCCs, are bounded from below by the PStress corresponding values and from above by the PStrain corresponding ones. Moreover, both Table 2 and Fig. 3 indicate that PStress frequency and EMCC results are closer to the 3D ones; it can then be concluded that they are more accurate than PStrain ones.

Table 1 3D transverse (x - z) bending frequencies of the smart cantilever beam

Mode		SC frequencies		OC frequencies		
3D	x - z bending	f_{SC} (Hz)	f_E (Hz)	$f_{\bar{D}}$ (Hz)	f_{NE} (Hz)	f_{EP} (Hz)
1	1	35.05	35.048	35.739	35.738	35.719
2	2	196.29	196.28	196.6	198.59	198.13
4	3	541.46	541.44	547.01	547.00	544.39
6	4	1058.3	1058.3	1066.6	1066.5	1058.8
8	5	1771.5	1771.4	1794.7	1794.7	1783.9
10	6	2658.4	2658.3	2687.3	2687.2	2665.1

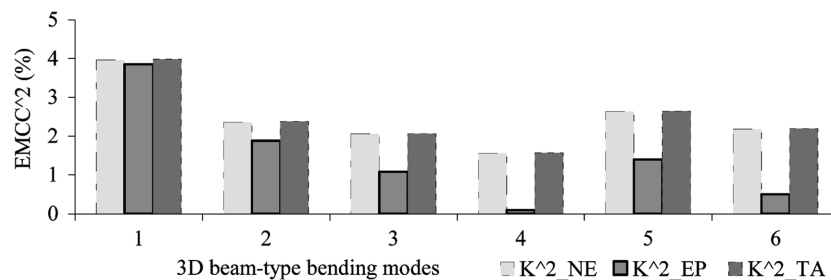


Fig. 2 3D first six transverse bending modes EMCC of the cantilever smart beam

Table 2 2D PStrain and PStress frequencies of the smart cantilever beam

Mode		PStrain frequencies		PStress frequencies	
3D	<i>x-z</i> bending	f_{SC} (Hz)	f_{EP} (Hz)	f_{SC} (Hz)	f_{EP} (Hz)
1	1	37.06	38.528	34.908	35.402
2	2	206.62	210.46	194.8	196.11
4	3	566.87	572.87	534.56	536.59
6	4	1099.4	1100.6	1037.1	1037.5
8	5	1825.1	1851.6	1721.0	1729.9
10	6	2707.4	2723.7	2554.0	2559.2

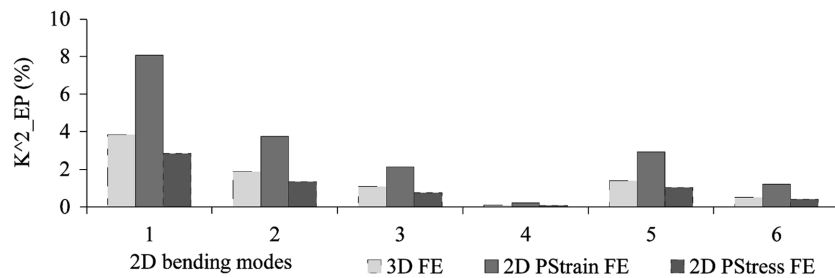


Fig. 3 2D PStrain and PStress first six bending modes EMCC of the cantilever smart beam

7. Conclusions

The most used practical (engineering) modeling approaches, such as the thermal analogy (TA) approach and the strain induced potential (IP) concept were discussed. Focus was made on their limitations and possible new solutions. Hence, the TA was extended from currently static actuation only to piezoelectric short-circuit (SC) and approximate open-circuit (OC) free-vibrations and electromechanical coupling coefficient (EMCC) evaluation. The revisit of the IP concept has shown that its SC free-vibrations problem is in fact the same as the newly defined OC TA one and that it is insensitive to SC/OC electric conditions. To avoid confusion, the EMCC correct evaluation from this concept has been clarified. On the other hand, two-dimensional (2D) plane strain (PStrain) and plane stress (PStress) modeling suitability of piezoelectric free-vibrations has been discussed. It was shown theoretically that 3D SC and OC frequencies and resulting EMCC should be bounded from above by their PStrain values and from below by their PStress ones.

The previous theoretically predicted results and their ANSYS FE validations on a typical piezoelectric smart structure benchmark confirm that:

- The TA approach can be used safely for SC and approximate OC free-vibrations analyses of piezoelectric smart structures. However, it should be kept in mind that it does not consider the EP constraint; this should be crucial for the EMCC.
- 3D frequencies and EMCCs are bounded from below by PStress results and from above by PStrain ones,
- PStrain results are higher than PStress, and overestimate 3D ones.
- The EP constraint affects more the EMCC evaluation than the frequencies; it decreases the former, in particular for higher modes.

These theoretical analyses and numerical FE results appeal for the following recommendations:

- The TA approach can be used safely for analyzing piezoelectric smart structures free vibrations, but care should be taken for its use in the EMCC evaluation since it does not consider the EP constraint which affects greatly the latter.
- Prefer 2D PStress analysis rather than PStrain one for the simulation of piezoelectric adaptive structures free vibrations when piezoelectric plate/shell FE models are not available or 3D ones are not cost-efficient.
- Apply the electrodes equipotential constraint on the unknown electric potential degrees of freedom for OC free-vibrations and sensing numerical analyses in particular when the EMCC has to be evaluated.

References

- Al-Ajmi, M.A. and Benjeddou, A. (2008), "Damage indication in smart structures using modal effective electromechanical coupling coefficients", *Smart Mater. Struct.*, **17**(6), 035023 (15p).
- Benjeddou, A. (2000), "Advances in piezoelectric finite element modeling of adaptive structural elements: a survey", *Comput. Struct.*, **76**(1-3), 347-363.
- Benjeddou, A. (2002), "Modelling of piezoelectric adaptive beam, plate and shell structures: some developments and results", *Proc. of the Sixth Int. Conf. on Computational Structures Technology*, B.H.V Topping and Z. Bitnar (Eds.), Civil-Comp Press, Stirling, Scotland, Paper 81. Invited Lecture.
- Benjeddou, A. (2004), *Modelling and simulation of adaptive structures and composites: current trends and future directions*, in *Progress in Computational Structures Technology*, B.H.V Topping and C.A. Mota Soares (Eds.), Saxe-Coburg Publications, Stirling, Scotland, Chapter 10, 251-280. Special Lecture.
- Benjeddou, A. (2008), *Piezoelectricity experimentation, modeling and simulation: common practices and realistic considerations*, in *Advances in Science and Technology*, Trans Tech Publications, Switzerland, **56**, 22-31. Invited Lecture.
- Benjeddou, A. and Ranger, J.A. (2006), "Use of shear-mode piezoceramics for structural vibration passive damping", *Comput. Struct.*, **84**(22-23), 1415-1425.
- Benjeddou, A., Trindade, M.A. and Ohayon, R. (1997), "A unified beam finite element model for extension and shear piezoelectric actuation mechanisms", *J. Intel. Mat. Syst. Str.*, **8**(12), 1012-1025.
- Brockmann, T.H., Lammering, R. and Yang, F. (2006), "Modelling and computational analysis of structures with integrated piezoelectric material", *Mech. Adv. Mater. Struct.*, **13**(5), 371-378.
- Chevallier, G., Ghorbel, S. and Benjeddou, A. (2008), "A benchmark for free-vibration and effective coupling of thick smart structures", *Smart Mater. Struct.*, **17**(6), 065007 (11p).
- Collet, M. and Cunefare, K.A. (2008), "Modal synthesis and dynamical condensation methods for accurate piezoelectric systems impedance computation", *J. Intel. Mat. Syst. Str.*, **19**(11), 1251-1269.
- Côté, F., Masson, P., Mrad, N. and Cotoni, V. (2004), "Dynamic and static modelling of piezoelectric composite structures using a thermal analogy with MSC/NASTRAN", *Compos. Struct.*, **65**, 471-484.
- Deü, J.F. and Benjeddou, A. (2005), "Free-vibration analysis of laminated plates with embedded shear-mode piezoceramic layers", *Int. J. Solids Struct.*, **42**(7), 2059-2088.
- Fernandes, A. and Pouget, J. (2003), "Analytical and numerical approaches to piezoelectric bimorph", *Int. J. Solids Struct.*, **40**, 4331-4352.
- Hagood, N.W., Chung, W.H. and von Flotow, A. (1990), "Modelling of piezoelectric actuator dynamics for active structural control", *J. Intel. Mat. Syst. Str.*, **1**(7), 327-354.
- Hagood, N.W. and von Flotow, A. (1991), "Damping of structural vibrations with piezoelectric materials and passive electrical networks", *J. Sound Vib.*, **146**, 243-268.
- Heyliger, P. and Brooks, S. (1995), "Free vibration of piezoelectric laminates in cylindrical bending", *Int. J. Solids Struct.*, **32**, 2945-2960.
- IEEE Inc. (1988), *Standard on Piezoelectricity*, ANS/IEEE Std 176-1987, USA.

- Jiang, J.D. and Li, D.X. (2008), "Finite element formulation for thermopiezoelectric elastic laminated composite plates", *Smart Mater. Struct.*, **17**, 015027 (13pp).
- Kim, D.K., Kim, H.I., Han, J.H. and Kwon, K.J. (2008), "Experimental investigation on the aerodynamic characteristics of a bio-mimetic flapping wing with macro-fiber composites", *J. Intel. Mat. Syst. Str.*, **19**(3), 423-431.
- Krommer, M. (2000), "An electromechanically coupled plate theory taking into account the influence of shear rotary inertia and electric field", *Mech. Res. Comm.*, **27**, 197-202.
- Krommer, M. (2003a), "The significance of non-local constitutive relations for composite thin plates including piezoelectric layers with prescribed electric charge", *Smart Mater. Struct.*, **12**, 318-330.
- Krommer, M. (2003b), "Piezoelectric vibrations of composite Reissner-Mindlin type plate", *J. Sound Vib.*, **263**, 871-891.
- Lin, M.W., Abatan, A.O. and Rogers, C.A. (1994), "Application of commercial finite element codes for the analysis of induced strain actuated structures", *J. Intel. Mat. Syst. Str.*, **5**, 869-875.
- Marinkovic, D., Köppe, H. and Gabbert, U. (2007), "Accurate modelling of the electric field within piezoelectric layers for active composite structures", *J. Intel. Mat. Syst. Str.*, **18**(5), 503-513.
- Poizat, C. and Benjeddou, A. (2006), "On analytical and finite element modeling of piezoelectric extension and shear bimorphs", *Comput. Struct.*, **84**(22-23), 1426-1437.
- Rahmoune, M., Benjeddou, A., Ohayon, R. and Osmont, D. (1998), "New thin piezoelectric plate models", *J. Intel. Mat. Syst. Str.*, **9**(12), 1017-1029.
- Shu, X. (2005), "Free vibration of laminated piezoelectric composite plates based on accurate theory", *Compos. Struct.*, **67**, 375-382.
- Thornburgh, R.P. and Chattopadhyay, A. (2001), "Electrical-mechanical coupling effects on the dynamic response of smart composite structures", *Proc. of the Smart Structures and Materials: Smart Structures and Integrated Systems*, L.P. Davis (Ed.), SPIE, **4327**, 413-424.
- Vel, S.S., Mewer, R.C. and Batra, R.C. (2004), "Analytical solution for the cylindrical bending vibration of piezoelectric composite plates", *Int. J. Solids Struct.*, **41**, 1625-1643.
- Wang, S.Y. (2004), "A finite element model for the static and dynamic analysis of a piezoelectric bimorph", *Int. J. Solids Struct.*, **41**, 4075-4096.
- Zhang, Z., Feng, C. and Liew, K.M. (2006), "Three-dimensional vibration analysis of multilayered piezoelectric composite plates", *Int. J. Eng. Sci.*, **44**, 397-408.

Appendix A: List of acronyms

1D	One-dimensional
2D	Two-dimensional
3D	Three-dimensional
BC	boundary conditions
DOF	Degrees of freedom
EMCC	Electromechanical coupling coefficient
EP	Equipotential
ESF	Extra shape functions
FE	Finite element
IF	Induced field
IP	Induced potential
NE	Non electroded
OC	Open circuit
PStrain	Plane strain
PStress	Plane stress
SC	Short circuit
SE	Stiffening effect
TA	Thermal analogy

Appendix B: 3D full and reduced OC elastic matrices

For a piezoelectric material polarized along its thickness (3rd material axis), the SC stiffness elastic, piezoelectric and blocked dielectric matrices of Eqs. (8,9) are:

$$[c^E] = \begin{bmatrix} c_{11} & c_{12} & c_{13} & 0 & 0 & 0 \\ c_{12} & c_{22} & c_{23} & 0 & 0 & 0 \\ c_{13} & c_{23} & c_{33} & 0 & 0 & 0 \\ 0 & 0 & 0 & c_{44} & 0 & 0 \\ 0 & 0 & 0 & 0 & c_{55} & 0 \\ 0 & 0 & 0 & 0 & 0 & c_{66} \end{bmatrix}^E \quad (\text{B1})$$

$$[e] = \begin{bmatrix} 0 & 0 & 0 & 0 & e_{15} & 0 \\ 0 & 0 & 0 & e_{24} & 0 & 0 \\ e_{31} & e_{32} & e_{33} & 0 & 0 & 0 \end{bmatrix}, \quad [\epsilon^S] = \begin{bmatrix} \epsilon_{11} & 0 & 0 \\ 0 & \epsilon_{22} & 0 \\ 0 & 0 & \epsilon_{33} \end{bmatrix}^S \quad (\text{B2})$$

Substituting these matrices in Eq. (37), provides the full OC elastic matrix (only non nil and upper triangle terms are shown):

$$[\epsilon_{p//z}^S] = \begin{bmatrix} 8.104 & 0 & 0 \\ 0 & 8.104 & 0 \\ 0 & 0 & 6.880 \end{bmatrix} \text{ (nF/m)} \quad (C3)$$

From these data, the full and reduced open-circuit (OC) matrices, as in Eqs. (B3, B4), can be obtained, respectively, as (only non nil terms are given):

$$[c_{p//z}^D] = \begin{bmatrix} 106.75 & 61.57 & 34.94 & & & \\ 61.57 & 106.75 & 34.94 & & & \\ 34.94 & 34.94 & 120.07 & & & \\ & & & 39.83 & & \\ & & & & 39.83 & \\ & & & & & 22.59 \end{bmatrix} \text{ (GPa)} \quad (C4)$$

$$[\bar{c}_{p//z}^D] = \begin{bmatrix} 106.75 & 61.57 & 34.94 & & & \\ 61.57 & 106.75 & 34.94 & & & \\ 34.94 & 34.94 & 120.07 & & & \\ & & & 21.10 & & \\ & & & & 21.10 & \\ & & & & & 22.59 \end{bmatrix} \text{ (GPa)} \quad (C5)$$

When the polarization is turned along axis 2 ($p//y$) (required in the two-dimensional (2D) plane strain (PStrain) and plane stress (PStress) analyses), above matrices of Eqs. (C1-C5) become, after the exchange of directions 3 and 2:

$$[c_{p//y}^E] = \begin{bmatrix} \mathbf{99.201} & \mathbf{50.778} & 54.016 & 0 & 0 & 0 \\ \mathbf{50.778} & \mathbf{86.856} & 50.778 & 0 & 0 & 0 \\ 54.016 & 50.778 & 99.201 & 0 & 0 & 0 \\ 0 & 0 & 0 & 21.10 & 0 & 0 \\ 0 & 0 & 0 & 0 & 22.593 & 0 \\ 0 & 0 & 0 & 0 & 0 & \mathbf{21.10} \end{bmatrix} \text{ (GPa)} \quad (C6)$$

$$[e_{p//y}] = \begin{bmatrix} 0 & 0 & 0 & 0 & 0 & 12.322 \\ -7.209 & 15.118 & -7.209 & 0 & 0 & 0 \\ 0 & 0 & 0 & 12.322 & 0 & 0 \end{bmatrix} \text{ (C/m}^2\text{)} \quad (C7)$$

$$[\epsilon_{p//y}^S] = \begin{bmatrix} 8.104 & 0 & 0 \\ 0 & 6.880 & 0 \\ 0 & 0 & 8.104 \end{bmatrix} \text{ (nF/m)} \quad (C8)$$

$$[c_{p//y}^D] = \begin{bmatrix} 106.75 & 34.94 & 61.57 & & & \\ 34.94 & 120.07 & 34.94 & & & \\ 61.57 & 34.94 & 106.75 & & & \\ \hline & & & 39.83 & & \\ & & & & 22.59 & \\ & & & & & 39.83 \end{bmatrix} \text{ (GPa)} \quad (\text{C9})$$

$$[\bar{c}_{p//y}^D] = \begin{bmatrix} \mathbf{106.75} & \mathbf{34.94} & 61.57 & & & \\ \mathbf{34.94} & \mathbf{120.07} & 34.94 & & & \\ 61.57 & 34.94 & 106.75 & & & \\ \hline & & & 21.10 & & \\ & & & & 22.59 & \\ & & & & & \mathbf{21.10} \end{bmatrix} \text{ (GPa)} \quad (\text{C10})$$

Under 2D PStrain electromechanical assumptions (Eqs. (60a,b)), SC and OC matrices of Eqs. (65) and (66), respectively, are:

$$[c_{P\text{Strain}}^E] = \begin{bmatrix} \mathbf{99.201} & \mathbf{50.778} & 0 \\ \mathbf{50.778} & \mathbf{86.856} & 0 \\ 0 & 0 & \mathbf{21.10} \end{bmatrix} \text{ (GPa)} \quad (\text{C11})$$

$$[c_{P\text{Strain}}^D] = \begin{bmatrix} \mathbf{106.75} & \mathbf{34.94} & 0 \\ \mathbf{34.94} & \mathbf{120.07} & 0 \\ 0 & 0 & \mathbf{21.10} \end{bmatrix} \text{ (GPa)} \quad (\text{C12})$$

It is worthy to mention that Eqs. (C11) and (C12) can be deduced from Eqs. (C6) and (C10), respectively, by applying the PStrain mechanical assumptions only (Eq. (60a)); i.e., by removing 3rd, 4th and 5th columns and rows of Eqs. (C6, C10).

Similarly, under 2D PStress electromechanical assumptions (Eqs. (68a,b)), SC and OC properties, as in Eqs. (72), (73) and (74), are respectively:

$$\bar{e}_{31} = -3.2836 \text{C/m}^2, \bar{e}_{33} = 18.8081 \text{C/m}^2, \epsilon_{33}^{-S} = 7.4043 \text{ nF/m} \quad (\text{C13})$$

$$[c_{P\text{Stress}}^E] = \begin{bmatrix} \mathbf{69.789} & \mathbf{23.129} & 0 \\ \mathbf{23.129} & \mathbf{60.864} & 0 \\ 0 & 0 & \mathbf{21.10} \end{bmatrix} \text{ (GPa)} \quad (\text{C14})$$

$$[c_{P\text{Stress}}^{-D}] = \begin{bmatrix} \mathbf{71.24} & \mathbf{14.79} & 0 \\ \mathbf{14.79} & \mathbf{108.64} & 0 \\ 0 & 0 & \mathbf{21.10} \end{bmatrix} \text{ (GPa)} \quad (\text{C15})$$

Eqs. (C14) and (C15) can be deduced from Eqs. (C6) and (C10), respectively, by applying the PStress mechanical assumptions only (Eq. (68a)). Besides, both SC and OC PStress stiffness terms of Eqs. (C14, C15) are lower than PStrain ones as in Eqs. (C11, C12) confirming the comments given in the text. Also, Eq. (C13) shows that the PStress transverse and longitudinal piezoelectric constants have decreased and increased, respectively while the dielectric one has increased.